NeuroImage: Clinical 49 (2026) 103944

Contents lists available at ScienceDirect

NeuroImage: Clinical

journal homepage: www.elsevier.com/locate/ynicl

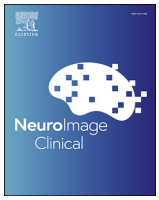

Striatal dopamine synthesis capacity in Parkinson's disease: Effects of age, sex, and body mass index in a large [^{18}F]fluorodopa PET cohort

Tuulia Malén [a,*], Jouni Tuisku [a], Marco Bucci [a,b], Severi Santavirta [a], Valtteri Kaasinen [c,d], Sakari Kaasalainen [a], Janne Isojärvi [a], Jarmo Hietala [a,e], Juha Rinne [a], Lauri Nummenmaa [a,f]

[a] Turku PET Centre, Turku University Hospital and University of Turku, Turku, Finland
[b] Division of Clinical Geriatrics, Center for Alzheimer Research, Department of Neurobiology, Care Sciences and Society, Karolinska Institutet, Stockholm, Sweden
[c] Clinical Neurosciences, University of Turku, Turku, Finland
[d] Neurocenter, Turku University Hospital, Turku, Finland
[e] Department of Psychiatry, University of Turku and Turku University Hospital, Turku, Finland
[f] Department of Psychology, University of Turku, Turku, Finland

ARTICLE INFO

Keywords:
Dopamine synthesis capacity
Positron emission tomography
Demographic effects
Parkinson's disease
Scanner effect
Bayesian modeling

ABSTRACT

Background: Positron emission tomography (PET) using radioligand [^{18}F]fluorodopa detects reduced striatal dopamine synthesis capacity in Parkinson's disease (PD) patients. Demographic factors such as sex and BMI are also associated with dopamine synthesis capacity. The combined contribution of demographic and clinical effects however remains elusive.

Material, aims, and methods: For this retrospective register-based study, we used baseline [^{18}F]fluorodopa PET data acquired at the Turku PET Centre between the years 1988–2016 with three scanners (Ecat 931, GE Advance, HRRT). The data involved 350 adult human subjects, including 132 healthy controls, and 218 PD patients. The primary aim was to simultaneously investigate the effects of PD, age, sex and BMI on regional dopamine synthesis capacity (influx rate constant Ki^{ref} quantified with Patlak in atlas-based regions of interest) using Bayesian linear regression. Secondary aims were to assess (1) interregional correlations of dopamine synthesis capacity, (2) association between regional presynaptic dopamine synthesis and postsynaptic dopamine type 2 receptor (D_2R) availability in subjects who also had a proximal [^{11}C]raclopride PET scan, and (3) scanner effects and atlas- versus MRI-based quantification approaches. We provide the mean dopamine synthesis brain maps of healthy controls and PD patients in NeuroVault.

Results: Dopamine synthesis capacity was drastically reduced in PD patients, decreased with age, increased with BMI, and higher in females versus males. Across regions, the capacity was positively correlated in both patients and controls. We observed support for positive correlation between the dopamine synthesis capacity and the D_2R in caudate nucleus. Scanner had a substantial influence on Ki^{ref} estimates. Atlas- and MRI-based normalization methods provide largely comparable Ki^{ref} estimates for most subjects.

Conclusions: Dopamine synthesis capacity is independently affected by PD and demographic factors and correlated between the striatal and thalamic regions in both controls and PD patients. Adjusting for scanner effects in multi-scanner datasets is recommended. When subject-specific MRI is unavailable, atlas-based normalization may be used with caution to prevent major data loss.

1. Introduction

Parkinson's disease (PD) is characterized by progressive degeneration of nigrostriatal dopaminergic neurons, leading to initially asymmetric motor symptoms and reduced striatal dopamine synthesis capacity detectable with [^{18}F]fluorodopa positron emission tomography (PET) (Kalia & Lang, 2015). [^{18}F]fluorodopa uptake is a measure of aromatic L-amino acid decarboxylase (AADC) activity reflecting dopamine synthesis capacity, and it reliably distinguishes patients with PD from healthy controls even at early disease stages (Kaasinen & Vahlberg, 2017).

Apart from the PD effect (Darbin, 2012), normal aging is also

* Corresponding author.
E-mail address: tukama@utu.fi (T. Malén).

https://doi.org/10.1016/j.nicl.2026.103944
Received 20 October 2025; Received in revised form 22 December 2025; Accepted 6 January 2026
Available online 7 January 2026

associated with gradual dopaminergic decline (Malén et al., 2022), consistently demonstrated for dopamine receptors and transporters, although evidence for changes in dopamine synthesis capacity is less consistent (Karrer et al., 2017). Potentially, males show reduced [^{18}F]fluorodopa uptake along age and compared to females (Laakso et al., 2002). Moreover, higher body mass index (BMI) has been associated with lower dopamine synthesis capacity (Janssen & Horstmann, 2022), while dopamine receptor availability is unaffected by BMI (Pak & Nummenmaa, 2023).

Previous [^{18}F]fluorodopa PET studies have been limited by modest sample sizes and restricted scope, focusing either on PD versus controls or on demographic effects in healthy subjects. The combined contribution of demographic influences and PD-related changes has not systematically been addressed. Furthermore, the extent to which dopamine synthesis capacity is coupled within striatal regions and with striatal dopamine receptor function in PD and controls remains unknown. Earlier evidence from healthy controls suggests a positive association between striatal dopamine synthesis capacity and type 2 dopamine receptor (D_2R) availability (Berry et al., 2018).

The aim of this study was to pool retrospective [^{18}F]fluorodopa data from a large (350 subjects) sample of subjects to simultaneously assess the effects of PD, age, sex, and BMI on striatal dopamine synthesis capacity. Secondary aims were to investigate: (1) interregional correlations of dopamine synthesis capacity, (2) association between dopamine synthesis and D_2R availability in subjects with dual-tracer scans, and (3) methodological factors including scanner effects and atlas- versus MRI-based quantification approaches. Our final aim was to provide the mean dopamine synthesis brain maps of healthy controls and PD patients in NeuroVault (https://neurovault.org).

2. Material and methods

2.1. Data

The data were baseline [^{18}F]fluorodopa PET images of 350 adult human subjects, including 132 healthy controls (65 males and 67 females), and 218 PD patients (134 males and 84 females) for whom sufficient demographic and imaging data, derived from an in-house database Aivo (https://aivo.utu.fi), were available. The scans were acquired at the Turku PET Centre between the years 1988–2016 with three different scanners (Ecat 931, GE Advance, HRRT, from oldest to newest at the site). See details for the original studies in the Supplementary Material (section **Publications whose data are used in the current study**).

The initial sample of 367 subjects was cut down to 350 after exclusion criteria were applied to 17 subjects as follows. One PD patient with prior thalamotomy, one with clinically undetermined parkinsonian syndrome after follow-up, and one with later determined drug-induced parkinsonism were excluded. These occurrences were found during retrospective data collection from the Finnish health care documentation by researchers with sufficient expertise in medicine and applicable permissions to access the data. We excluded seven subjects due to insufficient number of collected frames for reliable modeling (four or less within 15–60 min of the scanning), six with missing PET estimates from one or more regions of interest (ROI), and one with abnormally low signal intensity likely reflecting failed tracer injection and/or preprocessing error. After these exclusions, the total sample consisted of 350 subjects.

The age range of the subjects was 19–81 years. Body mass index (BMI) data were available for 220 subjects (BMI subsample, 63 % of the total sample), ranging from 17.8 to 43.8. We used at that time the current versions of the UK Parkinson's Disease Society Brain Bank clinical diagnostic criteria (Gibb & Lees, 1988), and the Movement Disorders Society's (MDS) clinical diagnostic criteria (Postuma et al., 2015). The controls were individuals recruited specifically for research purposes, and they had no history or current signs or symptoms of neurological disorders (excluding migraine). However, information on PD duration, motor symptom severity, medication use, smoking status, or handedness was not systematically available. From the total sample, the PD duration (median 12 years) from symptom onset was available for 18 subjects, while the information on medication was available for 11 patients (3 scanned with GE Advance, 8 with HRRT). However, a common protocol at the site has been withdrawal from medication (levodopa at least for 12 h; MAO-B inhibitors and dopamine agonists for 24 h) prior to imaging. Among the healthy controls, 14 individuals in the total sample (11 in the BMI subsample) were non-psychotic first-degree relatives of patients with schizophrenia. Descriptive statistics of the total sample and BMI subsample are summarized in Tables 1 and 2, respectively. Age and BMI distributions are shown in Fig. 1. Based on Wilcoxon and Kruskal-Wallis rank sum testing of the total sample (Table 1) and BMI subsample (Table 2) using R package stats (R Core Team, 2025), the age distribution varied by clinical status and scanner, but not sex. The BMI distribution varied by scanner, yet not clinical status or sex.

PET scan using [^{11}C]raclopride and taken within ±48 days from the [^{18}F]fluorodopa scan was available from 6 healthy controls and 26 PD patients. The subjects were included in the sample of our study on D_2R (Malén et al., 2024). The scanner for all 32 [^{18}F]fluorodopa and the matching 32 [^{11}C]raclopride images was Ecat 931. The median PD duration from symptom onset at [^{18}F]fluorodopa scan was 12 years in those 18 patients with the information available. Motor symptoms are estimated to occur with approximately 30% (while also higher estimations exist) degeneration of the dopamine nerves in substantia nigra (Cheng et al., 2010). Descriptive statistics of the subjects are given in Table 3. Based on t-testing using R package stats (R Core Team, 2025), the age distribution in this subsample did not vary by clinical status or sex.

2.2. PET image preprocessing

The [^{18}F]fluorodopa uptake was quantified using the Patlak method where the influx rate constant Ki^{ref} (Gjedde et al., 1991) was estimated using multiple time graphical analysis (Patlak & Blasberg, 1985) in regional and voxel level within 15 to 60 min by using the occipital cortex as reference region (Nurmi et al., 2001). Ki^{ref} is a slope that reflects the efficiency of AADC activity, i.e. dopamine synthesis capacity (Kaasinen & Vahlberg, 2017). Especially in regions with particularly low Ki^{ref}, the Patlak-based Ki^{ref} estimate may be below zero, possibly due to less signal with noisy filtered back projection reconstruction. In the total sample, there were altogether 29 negative Ki^{ref} estimates (4 in caudate, 1 in accumbens, 7 in putamen, and 17 in thalamus, involving observations of 20 subjects), of which 27/29 were acquired with Ecat 931 and 21/29 from PD patients. We did not remove observations with negative Ki^{ref} estimates to avoid a positive bias on the mean. The negative Ki^{ref} estimates could also stem from metabolites (Sossi et al., 2003). However, all subjects were administered 150 mg of carbidopa (a peripheral AADC inhibitor) an hour prior to tracer injection to minimize peripheral metabolism (Elsinga et al., 2006; Joutsa et al., 2015).

While the reconstruction of the radioactivity counts into PET images was not harmonized due to unavailable image-specific reconstruction algorithms, the image preprocessing and modeling were harmonized and performed with an in-house automated image analysis pipeline Magia (Karjalainen et al., 2020) running on MATLAB (The MathWorks Inc.). The pipeline included frame-by-frame realignment of PET images. The rate of dopamine synthesis can be measured by quantifying the accumulation of [^{18}F]fluorodopa in the striatum (Volkow et al., 1996). The data were analyzed in striatal regions of interest (ROIs); caudate nucleus later referred to as caudate, nucleus accumbens later referred to as accumbens, and putamen, as well as in thalamus. Bilateral ROIs were defined using Harvard-Oxford atlas, which was transformed into subject native space using an in-house created PET-template. These atlas-derived ROIs were used in the primary analyses because MRI data were not available for all participants.

Table 1
Demographic and imaging characteristics of the total sample (n = 350). HC = healthy controls, PD = patients with Parkinson's disease, SD = standard deviation. Scanner column shows the number of subjects imaged with each scanner.

Group	Age (years)			Sex		Scanner		
	Mean	SD	Range	Male	Female	Ecat 931	GE Advance	HRRT
HC (n = 132)	46.2	15.5	19.5–79.3	65	67	87	27	18
PD (n = 218)	61.7	10.4	27.2–81.7	134	84	96	102	20

Table 2
Demographic and imaging characteristics of the subsample of subjects with BMI information available (BMI subsample, n = 220, 63 % of the total sample). HC = healthy controls, PD = patients with Parkinson's disease, SD = standard deviation. Scanner column shows the number of subjects imaged with each scanner.

Group	Age (years)			Sex		BMI			Scanner		
	Mean	SD	Range	Male	Female	Mean	SD	Range	Ecat 931	GE Advance	HRRT
HC (n = 94)	45.5	15.3	19.5–79.3	46	48	25.3	3.5	17.8–38.8	52	26	16
PD (n = 126)	62.8	10.0	33.0–79.7	78	48	26.2	3.9	18.7–43.8	15	101	10

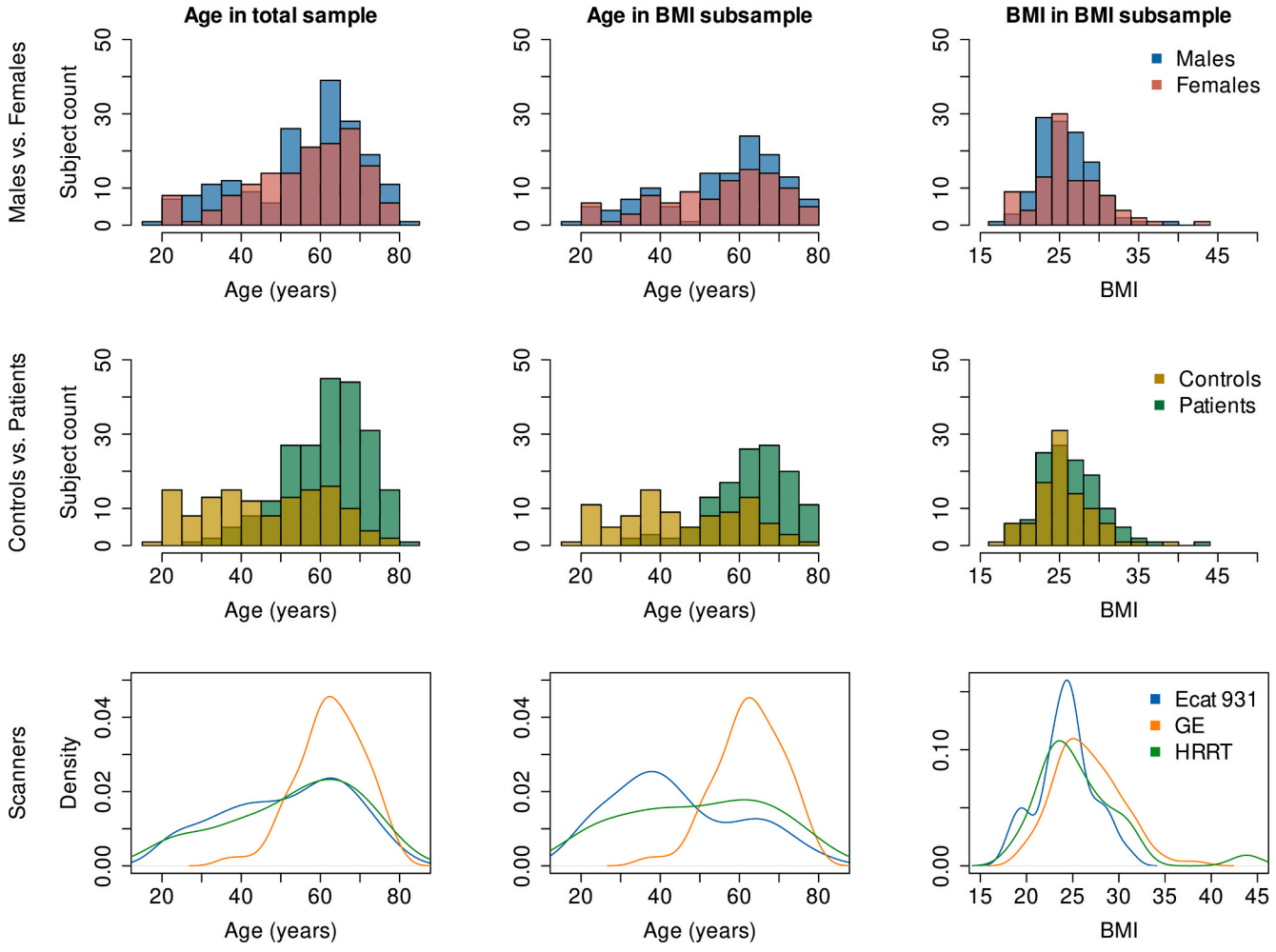

Fig. 1. Age and BMI histograms and density plots of the total sample and the subsample of subjects with BMI information available (BMI subsample, n = 220, 63 % of the total sample). The darker shades of red and yellow are overlapping with blue and green, respectively. GE = GE Advance. (For interpretation of the references to colour in this figure legend, the reader is referred to the web version of this article.)

Cases with structural MRI data available (n = 45, including 22 healthy controls and 23 PD patients) were also preprocessed independently using subject-specific MRI for spatial normalization. The preprocessing involved co-registration of MRI and PET images, and anatomical ROI extraction using FreeSurfer (Fischl, 2012) (version 7.2.0, https://surfer.nmr.mgh.harvard.edu/). For validation purposes, we compared the Ki^{ref} estimates derived from the atlas- and MRI-based normalization methods and estimated the main effects of age, sex, clinical status and scanner on (1) atlas-based and (2) MRI-based regional Ki^{ref} in the sample (n = 45). BMI effects were not estimated, as BMI was not available for all subjects. The one-tailed (greater) Pearson correlation between the Ki^{ref} estimates of the two alternative methods was 0.57

Table 3
Demographic and clinical characteristics of the subsample of subjects with proximal (maximum of 48 days apart) [^{18}F]fluorodopa and [^{11}C]raclopride scans available (n = 32). HC = healthy controls, PD = patients with Parkinson's disease, SD = standard deviation, NA = not applicable. Duration = Parkinson's disease duration from symptom onset of 18 patients with the available information. BMI is not given in the table, as it was available only for a few subjects. The table shows information at [^{18}F]fluorodopa scan.

Group	Age (years)			Sex		Duration (years, n = 18)		
	Mean	SD	Range	Male	Female	Mean	SD	Range
HC (n = 6)	60.6	7.0	51.2–72.2	2	4	NA	NA	NA
PD (n = 26)	58.8	12.8	34.2–81.7	15	11	11.9	7.7	1–29

(Spearman 0.69) in caudate, 0.13 (Spearman 0.40) in accumbens, 0.79 (Spearman 0.79) in putamen, and 0.46 (Spearman 0.45) in thalamus. The Pearson and Spearman correlations were statistically significant (p-values <= 0.001), except in accumbens. More details of the validation in Supplementary Material section **Comparison of atlas- and MRI-based Ki^{ref} estimates**. The uptake of [^{11}C]raclopride was quantified as described in our previous D_2R study (Malén et al., 2024).

2.3. Statistical analysis

To manage, analyze and visualize our data, we used MATLAB (The MathWorks Inc.), MRIcroGL (Rorden, 2025), and R (R Core Team, 2025) in RStudio (Posit team, 2023), including the packages data.table (Dowle, 2023), tidyr (Wickham, 2021), dplyr (Wickham et al., 2023), stringr (H. Wickham, 2022), reshape2 (Wickham, 2007), scales (Wickham and Dana, 2022), ggplot2 (Wickham, 2016), gridExtra (Auguie, 2017), ggdist (Kay, 2023a), patchwork (Pedersen, 2024), and tidybayes (Kay, 2023b).

For statistical analyses, mean Ki^{ref} estimates across hemispheres were used, as atlas-based normalization may not adequately capture subject-specific asymmetry. To ensure that potential lateralization effects were not overlooked, hemispheric differences were assessed in the subset with MRI-based Ki^{ref} estimates derived separately for left and right ROIs. Results supporting the validity of mean hemispheric estimates are presented in the Supplementary Material (section **Lateralization of Ki^{ref} estimates**).

2.3.1. Modeling of age, sex, BMI, PD, and scanner effects

We conducted Bayesian linear regression modeling using the R package brms (Bürkner, 2017, 2018, 2021) utilizing RStan (Stan Development Team, 2023). We ran the models separately for each ROI (caudate, accumbens, putamen, and thalamus). In the regional models, we estimated the fixed, population-level main effects of standardized age (slope), sex (difference between males and females), standardized BMI (slope), and PD (difference between PD patients and healthy controls) on standardized Ki^{ref}.

Despite calibration and standardization, different PET scanners used for each study may induce variation in the data, because the scanners differ in their properties, such as sensitivity and resolution, which may affect the acquired Ki^{ref} estimate. To address this potential variation, we also estimated the fixed (population-level) main effect of scanner on the standardized Ki^{ref}, as we wanted to estimate the scanner effect, as well as the effects of age, sex, BMI, and PD independently of the scanner.

We wanted to maximize the number of subjects in the modeling. Thus, we initially estimated the effects of age, sex, PD, and scanner in the total sample, but validated these effects also in the BMI subsample. The fixed effect of BMI was estimated only in the subsample where BMI was known.

In the Bayesian modeling, a prior probability distribution (prior) is given to each parameter in the model (McElreath, 2020). Each prior is updated with the data, resulting in a posterior distribution (posterior) that describes the probability distribution of the parameter (McElreath, 2020). In the regression modeling, we were interested in the posteriors for the regression coefficients of our fixed effects. Primarily, we set normal prior with expected value of 0, and standard deviation (SD) of 1 for the regression coefficients for age, sex, BMI, clinical status of the subject as PD patient or healthy control, and scanner, and used the default priors of brms for the remaining parameters.

To assess the effect of the chosen priors, we ran separate regional models using alternative priors that were assigned to the regression coefficients of BMI, sex, and the clinical status of the subject as PD patient or healthy control. The alternative priors for BMI, sex and PD were normal distributions weighting negative association (expected value: −1, SD: 0.5). The alternative prior specification was based on previous findings of lowered dopamine synthesis capacity in high BMI (Janssen & Horstmann, 2022), in males versus females (Laakso et al., 2002), and in PD patients versus healthy controls (e.g. Cropley et al., 2008; Pavese et al., 2011; Samii et al., 1999). Using alternative priors did not substantially change the findings. Normality and homoscedasticity of the modeling residuals suggest that the assumptions of the linear regression model are met, and that the model fits the data sufficiently. Assessing the residuals, we did not observe clear violations of normality nor homoscedasticity. More details of the diagnostics, including the modeling with alternative priors and the assessment of residuals, are given in the Supplementary Material (section **Model diagnostics**).

In the primary modeling, we calculated the age effect on Ki^{ref} for males and females together. To assess possible sex-dependency in the age-effect, we estimated the effect of age for males and females independently (fixed interaction of age and sex) in separate regional models.

In the primary regression modeling, we forced the associations between continuous predictors (age and BMI) and the dependent variable (Ki^{ref}) as slopes (straight lines). To assess whether the linear function adequately approximates the age and BMI effects, we ran separate regional models allowing nonlinearity in these effects.

The primary analyses estimated the effects of age, sex, and BMI together for healthy controls and PD patients. Additionally, we estimated the demographic effects on both the regional [^{18}F]fluorodopa (BMI subsample), and [^{11}C]raclopride (dual-tracer subsample) data, limiting the samples to PD patients.

We specified each regression model to run with four chains (Markov chain Monte Carlo, MCMC), and each chain was defined with 4000 iterations including 1000 warm-ups. Otherwise, the default specifications of brms were applied, except for the models allowing nonlinear effects, for which adapt-delta and maximum treedepth were modified to facilitate model convergence. Using these model fitting specifications, the models showed neither divergent transitions nor Rhats > 1, supporting sufficient model convergence (Vehtari et al., 2021). The R syntax for running the regression models is presented in the Supplementary Material (**R syntax for the regression models**).

2.3.2. Interregional correlations of Ki^{ref}

We analyzed interregional associations in Ki^{ref} separately in healthy controls and in PD patients in the total sample (n = 350). The Pearson correlations were analyzed separately for each scanner to avoid confounding effect of scanner. We tested whether the Ki^{ref} was normally distributed separately in healthy controls and PD patients within each scanner and each ROI using Shapiro-Wilk testing (significance level 0.01) in R package stats (R Core Team, 2025). Most of the tests (15/24) did not conflict with the null-hypothesis of normally distributed data, and we decided to estimate the correlation using (two-sided) Pearson

correlation with default specification of cor.test function in R package stats (R Core Team, 2025). We used original scale and not standardized Ki^{ref} estimates, as standardization here does not facilitate the interpretation of the findings similarly as in the regression modeling.

2.3.3. The relationship between striatal dopamine synthesis and D_2R availability

For the 32 subjects with baseline [^{18}F]fluorodopa and [^{11}C]raclopride scans conducted less than 48 days apart, we calculated the Pearson correlation (two-tailed testing) between [^{18}F]flurodopa Ki^{ref} and [^{11}C]raclopride binding potential (BP_{ND}) estimates, to assess the baseline link between regional dopamine synthesis capacity and D_2R receptor availability. Based on Shapiro-Wilk testing (significance level 0.01), the regional Ki^{ref} and BP_{ND} estimates did not conflict with the null-hypothesis of normally distributed data (except in thalamus). The relationship between Ki^{ref} and BP_{ND} was visually assessed not only for the subjects together but also separately for healthy controls and PD patients to give more insight on whether the relationship differs between the groups. In the assessment altogether, we used the original scale estimates.

3. Results

3.1. Group-differences in Ki^{ref}

Regional Ki^{ref} estimates (Fig. 2), and the group-specific whole-brain maps for mean Ki^{ref} (Fig. 3) demonstrate differences between healthy controls and PD patients. The ROI-specific coefficient of variation -maps show that the variation of Ki^{ref} estimates is greatest in thalamus (Fig. 3). Scanner-specific distributions are shown in Fig. 4.

3.2. The effects of demographic factors, PD, and scanner

Regression models were used to estimate the effects of age, sex, BMI, PD, and scanner on Ki^{ref}. The findings from the three model types – (1) effects of age, sex, PD, and scanner in the total sample, (2) the same effects in the BMI subsample, and (3) the same effects and the additional BMI effect in the BMI subsample – were essentially the same.

Ki^{ref} was lower in PD patients compared to healthy controls across striatal ROIs. Ki^{ref} also declined consistently with increasing age, and females had higher Ki^{ref} than males. Finally, Ki^{ref} estimates were systematically higher with newer scanners (GE Advance and particularly HRRT) compared to the reference scanner (Ecat 931).

In the BMI subsample, these effects were amplified (females > males, PD < controls, Ecat 931 < GE Advance < HRRT). Notably, the PD effect in the thalamus differed between analyses: positive in the total sample (PD > controls) but negative in the BMI subsample (PD < controls) with both model types (with and without the BMI effect). This discrepancy likely reflects sample composition. Of the 130 subjects excluded from the BMI subsample, 116 (89 %) were scanned with the oldest device (Ecat 931). Thus, the BMI subsample was enriched for higher-quality data (only 30 % scanned with Ecat 931), reducing scanner-related noise. BMI showed a modest positive association with striatal Ki^{ref}. Adding BMI as a predictor did not materially alter PD effects.

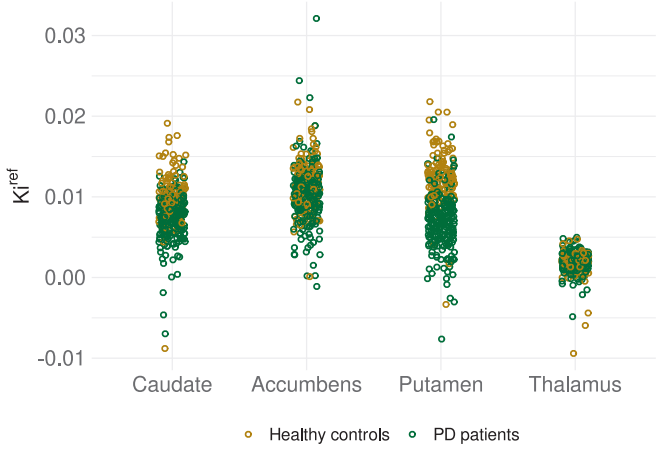

Fig. 2. Regional Ki^{ref} estimates in healthy controls and PD patients in the total sample (n = 350).

We therefore considered the BMI subsample models including BMI effect as the most reliable and present the results of these primary models in Table 4 and Fig. 5. Results from the other models are provided in the Supplementary Material (section **The effects of age, sex, PD, and scanner in the total sample and their validation in the BMI subsample**).

3.3. Interaction of age and sex

We assessed the age-effect separately in males and females (see details in Supplementary Material section **Interaction of age and sex**). These models suggested that the effect of age on Ki^{ref} was negative and roughly of a same magnitude in males and females, comparable to the observed age effects estimated for the males and females together. In accumbens, the negative age-effect was observed in females but not in males.

3.4. Linearity assessment of the age and BMI effects

We estimated the possible nonlinearity of the continuous effects of age and BMI (see details in Supplementary Material section **Linearity assessment of the age and BMI effects**). Due to uncertainty indicated by wide posterior intervals in the modeling estimates, the possible nonlinearity was difficult to assess, particularly at the ends of the age and BMI ranges. However, there was subtle support for nonlinear relationship between age and Ki^{ref} particularly in caudate and accumbens, suggesting a positive or nonexistent effect until the age of around 50 and a negative effect onwards. We did not see clear support for nonlinear BMI effect in any ROI.

3.5. Demographic effects in PD patients

As a complementary analysis, we estimated the demographic effects on [^{18}F]fluorodopa and [^{11}C]raclopride uptake in PD patients alone. Regarding [^{18}F]fluorodopa data, we observed a negative age effect (striatum and thalamus), and positive BMI effect (striatum) on regional Ki^{ref}, aligned with the analyses including healthy controls. The effect of sex was not apparent in PD patients. The effects of age and sex on regional [^{11}C]raclopride BP_{ND} were uncertain, indicated by the wide posterior intervals of the small sample. See more details of the analyses and findings in Supplementary Material (section **Demographic effects in PD patients**).

3.6. Interregional correlation of Ki^{ref}

The interregional Ki^{ref} Pearson correlations separately in healthy controls and PD patients within each scanner are given with sample sizes in Fig. 6. Based on Pearson correlation, particularly with the newer scanners HRRT and GE Advance, Ki^{ref} estimates were positively correlated across ROIs in both healthy controls and PD patients. The correlations appear stronger in newer scanners for both subject groups.

3.7. Relationship between striatal dopamine synthesis capacity and the D_2R availability

The comparison of the [^{18}F]fluorodopa Ki^{ref} and [^{11}C]raclopride BP_{ND} is shown in Fig. 7. Based on the figure and the Pearson correlation analyses, we did not observe clear support for overall link between

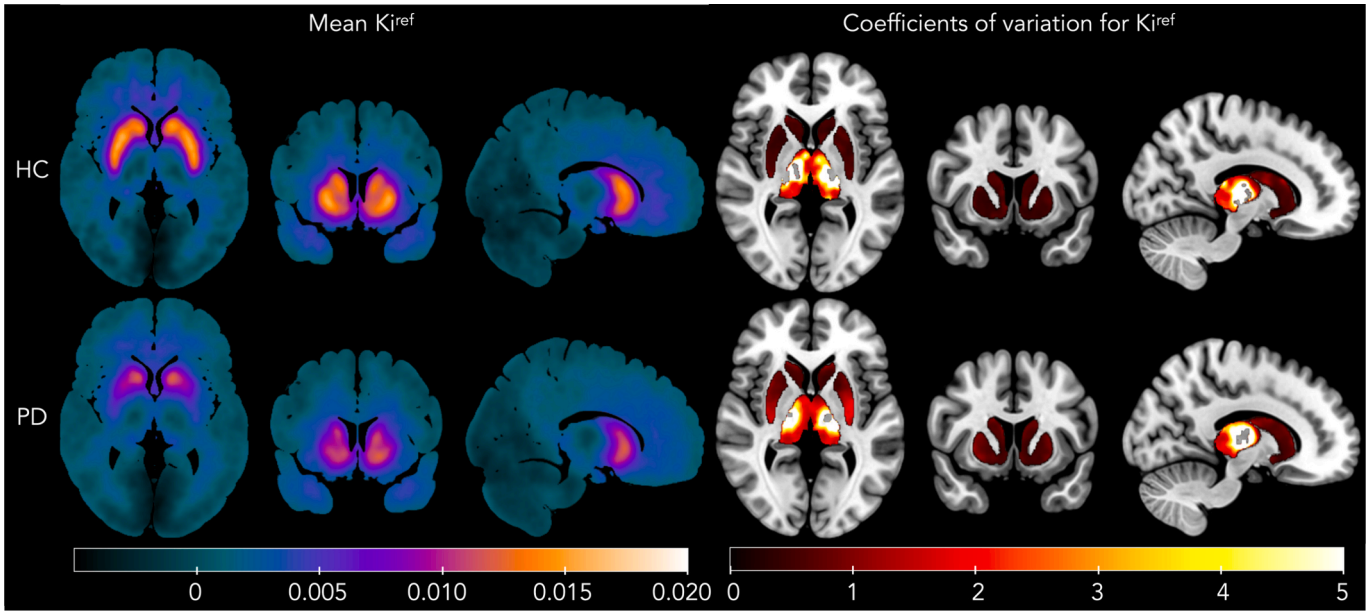

Fig. 3. Maps of the Ki^{ref} estimates across healthy controls (HC, n = 132) and Parkinson's disease patients (PD, n = 218) in the total sample (n = 350), using images normalized on MNI space. Left: Mean Ki^{ref}. Right: Coefficients of variation (standard deviation / mean) for Ki^{ref} within the regions of interest (Harvard-Oxford atlas masks). Each map is presented on an MNI template.

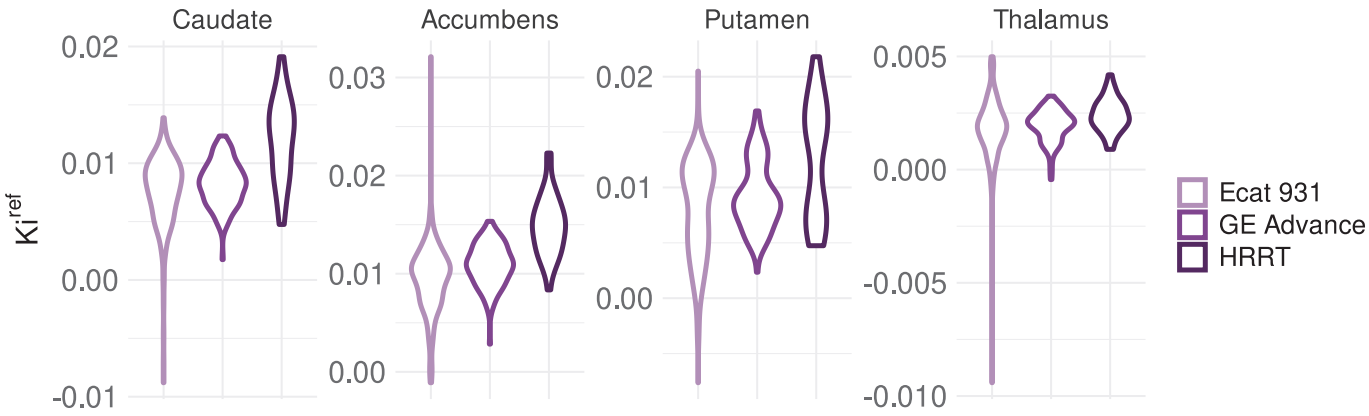

Fig. 4. Distributions of scanner-specific Ki^{ref} estimates in the total sample (n = 350).

Table 4
Effect sizes for age, sex, BMI, PD, and scanner type on regional Ki^{ref} in the BMI subsample (n = 220), expressed as posterior medians for regression coefficients on original scale, * 95% posterior interval did not cross zero. In parenthesis: For the continuous effects of age and BMI, the effect size is given as a percentage of mean regional Ki^{ref} across the sample. For the categorical effects of sex, PD, GE Advance, and HRRT, the effect size is given as a percentage of mean regional Ki^{ref} in the reference category (females, healthy controls, Ecat 931, and Ecat 931 respectively).

ROI	Age	Sex	BMI	PD	GE advance	HRRT
	per 15 years	males vs females	per 4 units	patients vs controls	vs Ecat 931	vs Ecat 931
Caudate	−0.0008* (9 %)	−0.0007* (8 %)	0.0003* (3 %)	−0.002* (21 %)	0.002* (22 %)	0.005* (56 %)
Accumbens	−0.0004* (4 %)	−0.0007* (6 %)	0.0003 (3 %)	−0.002* (13 %)	0.002* (20 %)	0.005* (50 %)
Putamen	−0.0005* (5 %)	−0.0007* (7 %)	0.0002 (2 %)	−0.005* (41 %)	0.003* (25 %)	0.004* (39 %)
Thalamus	−0.0002* (8 %)	−0.0002* (11 %)	< 0.00001 (0.4 %)	−0.0003* (15 %)	0.0006* (39 %)	0.0008* (50 %)

regional Ki^{ref} and BP_{ND}, although the positive correlation was statistically significant in caudate. The correlation was 0.48 (p = 0.006) in caudate, 0.25 (p = 0.16) in accumbens, 0.013 (p = 0.94) in putamen, and −0.007 (p = 0.97) in thalamus. Given the small sample size, especially for healthy controls, these results should be interpreted with caution.

4. Discussion

As expected, PD patients had lower dopamine synthesis capacity compared to healthy controls in the striatum and thalamus. Synthesis capacity also declined through age (striatal ROIs and thalamus), increased as a function of BMI (striatal ROIs), and the capacity was higher for females than males. The dopamine synthesis capacity was positively correlated across regions both in healthy controls and in PD

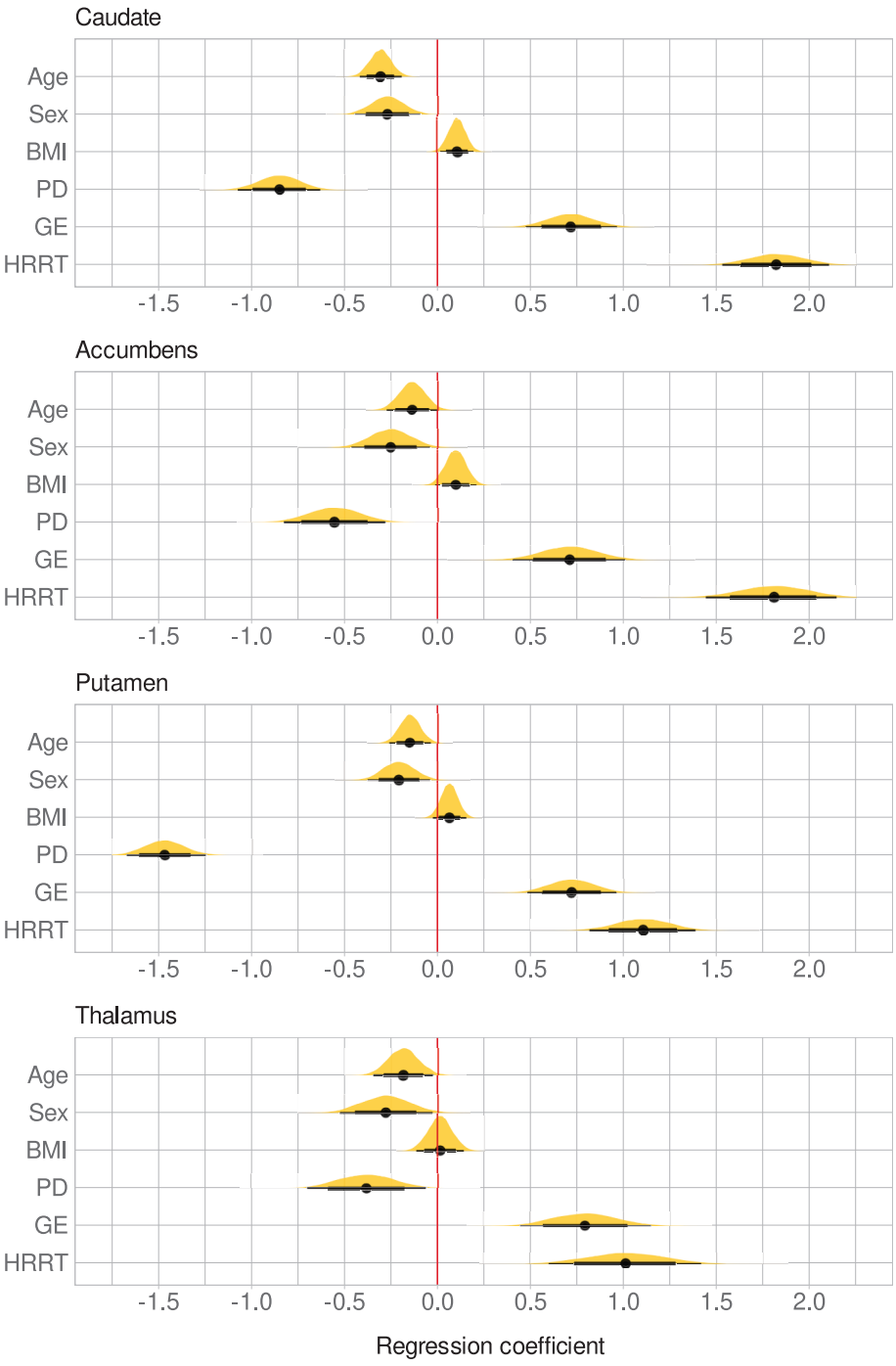

Fig. 5. Main effects of age, sex (males versus females), BMI, PD (PD patients versus healthy controls), and scanner (each scanner versus Ecat 931, GE = GE Advance) on Ki^{ref} in the BMI subsample (n = 220). The figure shows posterior distributions with medians (point) and intervals (95 % thin and 80 % thick line) on a standardized scale.

patients. Only in caudate, there was support for a positive correlation between dopamine synthesis capacity and D_2R availability when PD patients and healthy subjects were assessed together. Based on our data involving three different PET cameras, the scanner induces variation in the data, which should be adjusted for when analyzing Ki^{ref} estimates from different devices. Atlas- and MRI-based normalization methods however produced comparable Ki^{ref} estimates for most subjects.

4.1. Dopamine synthesis capacity, Parkinson's disease and demographic factors

Overall, the dopamine synthesis capacity was substantially lower in PD patients versus healthy controls, and the effect was greater than the demographic effects of age, sex, and BMI. Effect of PD on dopamine synthesis was particularly prominent in the striatal ROIs (putamen > caudate > accumbens). The PD related decline in the striatal dopamine synthesis is undebated (Kaasinen & Vahlberg, 2017), yet our findings support the theory of putamen-caudate-accumbens gradient of dopamine depletion (de la Fuente-Fernández, 2012) and highlight that the

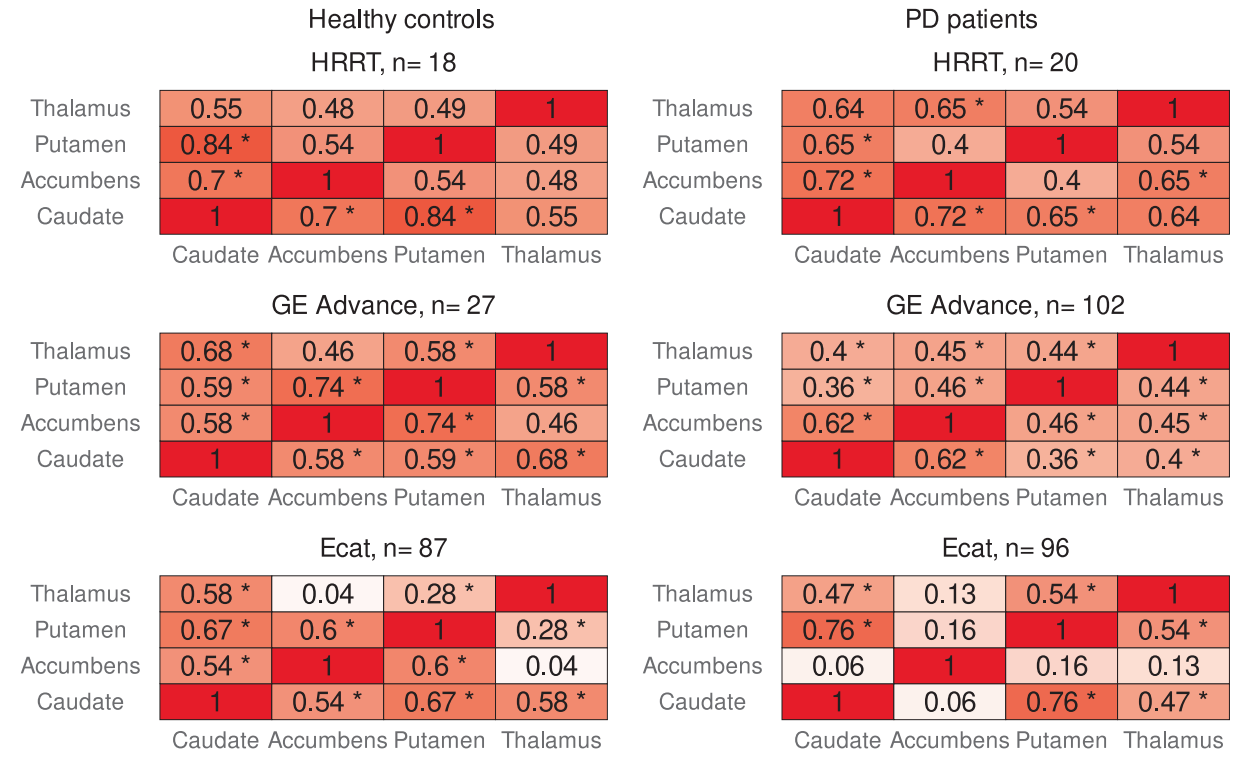

Fig. 6. Interregional Ki^{ref} Pearson correlations with sample sizes (n) in the total sample (n = 350). The table shows point estimates and the p-values of <0.01 (*). PD= Parkinson's disease.

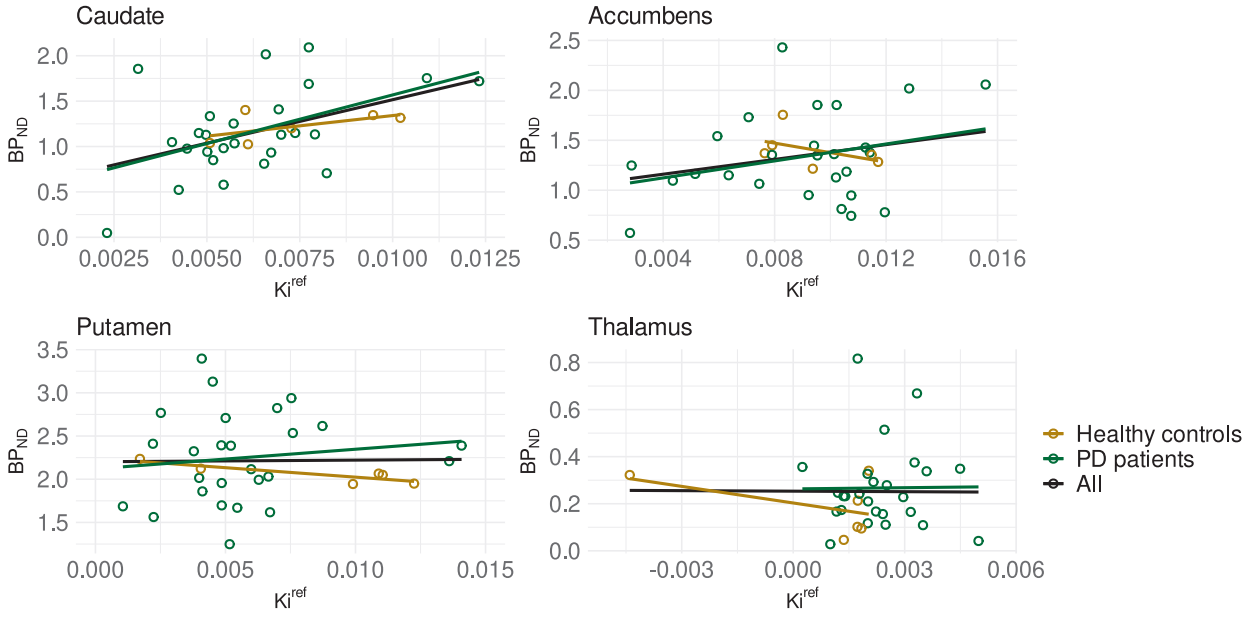

Fig. 7. Association between the [^{18}F]fluorodopa Ki^{ref} and [^{11}C]raclopride BP_{ND} in 32 subjects (6 healthy controls, 26 PD patients) in each ROI. The colored lines represent linear fits separately and together for the subject groups.

magnitude of the PD effect measurably exceeds the demographic effects. Dopamine synthesis capacity decreased with age in the combined sample of healthy controls and PD patients, in PD patients alone, as well as both in males and females. However, our data suggested that the decline may appear not until later adulthood (approximately at the age of 50), possibly contributing to cognitive (Karrer et al., 2017) and motor (Darbin, 2012) aging. The nonlinearity of the age effect (positive or nonexistent until negative in later adulthood) may have been overlooked in prior studies concluding correlation-based sex-dependency (Laakso et al., 2002), absence, or inconsistency of the age effect (Karrer et al., 2017). Overall, females had higher dopamine synthesis capacity than males in the striatum and thalamus, in line with an earlier analysis with possibly dependent, yet smaller sample from the site (Laakso et al., 2002). Consistently, in a study with [^{11}C]raclopride PET, females showed lower D_2R affinity than males, concluded to support higher endogenous striatal dopamine concentration in females versus males (Pohjalainen et al., 1998). In PD patients alone, unlike in the combined sample, there was no clear support for sex-difference in dopamine

synthesis capacity, possibly explained by the age-related reduction in neuroprotective estrogen (Haaxma et al., 2007; Lee et al., 2015).

A recent qualitative review (Janssen & Horstmann, 2022) supported negative association of BMI and dopamine synthesis in striatal subregions, based on three partial correlation studies with the sample sizes of 60 (Lee et al., 2018), 16 (Wallace et al., 2014), and 15 (Wilcox et al., 2010). We utilized these findings in our additional analysis by applying an alternative prior placing higher probability for negative than positive association between BMI and dopamine synthesis capacity. However, even with the alternative prior, our sample of two hundred subjects showed subtle support for a positive (although not sure if linear throughout the BMI range of 18–44) link between dopamine synthesis capacity and BMI in the striatal regions, while no link in thalamus, also when restricted to PD patients. Taken these conflicting findings together, the relationship between BMI and dopamine synthesis capacity does not appear strong.

4.2. Interregional correlations in dopamine synthesis capacity

To our knowledge, this is the first study to establish significant interregional correlations of dopamine synthesis capacity within striatal and thalamic regions in these groups. High correlation coefficients indicate that individuals with relatively low Ki^{ref} in one region also showed low Ki^{ref} in the remaining regions. These findings, thus, suggest that, in this mixed cohort, also PD is associated with a relatively uniform dopamine synthesis capacity across striatal subregions. However, because detailed information on disease stage was not systematically available, it is possible that very early PD shows considerably more regionally selective vulnerability. Altogether, the interregional correlations appeared stronger in newer scanners, which could reflect improved signal detection capabilities and the subsequent effects of smoothing and partial volume effects leading to stronger apparent correlations between adjacent regions.

4.3. Coupling of presynaptic dopamine synthesis and postsynaptic D_2R

In our dual-tracer subsample (n = 32), which consisted mainly of PD patients (81%) and was largely representative of later-stage disease (median 12 years from symptom onset), we did not observe clear support for overall link between regional dopamine synthesis capacity and D_2R availability, although their positive correlation was statistically significant in caudate. Heterogeneity in medication status of the patients may explain the absence of stronger correlations. However, a common protocol at the site has been withdrawal from medication (levodopa at least for 12 h; MAO-B inhibitors and dopamine agonists for 24 h). Positive correlation would suggest that, at advanced stages, presynaptic and postsynaptic dopaminergic markers decline in parallel.

Previous studies indicate that the relationship between these markers is dynamic and stage-dependent. In early PD, reduced dopamine synthesis capacity associates with higher [^{11}C]raclopride uptake possibly explained by (1) compensatory receptor upregulation (Kaasinen et al., 2021) and/ or (2) decreased receptor occupancy (Cumming et al., 2002) due to diminishing endogenous dopamine. Supporting compensatory upregulation, specifically the D_2R density is increased in putamen of patients with early PD (Rinne et al., 1995). The phenomenon is transient, typically lasting for the first four years after motor symptoms onset (Kaasinen et al., 2021). With progression, both synthesis capacity and receptor availability decline (Antonini et al., 1995), while pharmacological treatments may further influence the correlations through increased competition with endogenous dopamine (Thobois et al., 2004). Our findings therefore align with prior evidence that the increase in D_2R availability observed in early PD gives way to coupled downregulation of the synthesis and available receptors in later disease stages. However, the small sample size and imbalance between patients and controls precule definitive conclusions. Larger stage-stratified studies are required to clarify the trajectory of this relationship across the disease course.

4.4. Scanner affects the dopamine synthesis capacity measures using [^{18}F]fluorodopa PET

Scanner contributed to the regional measures of the dopamine synthesis capacity using [^{18}F]fluorodopa PET. The device order from highest to lowest Ki^{ref} estimates was HRRT > GE Advance > Ecat 931. It is recommended to adjust for the scanner effect when analyzing data acquired with different scanners. Here, we adjusted for the scanner by estimating the effects of interest independently of the scanner and the interregional correlation within each scanner. There are also other methods, such as data harmonization by scanner (Fortin et al., 2017; Lövdal et al., 2025). However, if the subject-related data is highly dependent on the device (e.g. all patients scanned with one device and healthy controls with another), careful consideration on how to adjust for the scanner is required to avoid confounds (McElreath, 2020).

4.5. Atlas-based spatial normalization can be used with caution to avoid great data loss due to missing MRIs

When individual-level structural MRI is not available, the data can be spatially normalized using common PET-atlas. Strong correlations between the Ki^{ref} estimates from the two methods were observed primarily in the putamen, and scanner-related differences appeared more pronounced for atlas-based normalization. The noise could possibly be reduced by adjusting for the scanner, which was not assessed here due to limited scanner-representation in the sample. Although MRI-based normalization should remain the preferred approach, the atlas-based normalization may be worth applying to avoid great data loss due to missing MRIs, particularly when the sample size is sufficient to cover the possible noise in the data. Nevertheless, whenever both MRI- and atlas-based estimates are available, their agreement should be evaluated to ensure the robustness of findings in future datasets.

5. Limitations

Clinical information, such as disease duration, medication status (except temporary withdrawal), and symptom severity was not systematically available, challenging the interpretation of our findings. The dual-tracer subsample used to examine the relationship between dopamine synthesis capacity and D_2R availability was small (n = 32) and predominantly composed of PD patients, limiting generalizability.

The retrospective dataset spanned three decades and multiple PET scanners, introducing technical heterogeneity despite statistical adjustment. Possibly, several different reconstruction algorithms were used for the scanners, which might have contributed to the observed effects. Although the reconstruction of the radioactivity counts into PET images was not harmonized due to unavailable image-specific reconstruction algorithms, the preprocessing of the PET data was harmonized and automatized using an in-house image analysis pipeline Magia (Karjalainen et al., 2020) running on MATLAB (The MathWorks Inc.). Most Ki^{ref} estimates were based on atlas-based normalization rather than subject-specific MRI, which may have added noise to the measurements. Adjusting for the scanner type could potentially have decreased the noise in the comparison of the spatial normalization methods, yet our sample was limited for such adjustment.

Finally, an alternative prior assigned in the regression modeling for the effect of sex was based on a sample (Laakso et al., 2002) that possibly, yet only partially, overlapped with our data. However, we made our primary conclusions from models that were not using the alternative prior.

6. Conclusions

PD significantly reduces striatal dopamine synthesis capacity.

Demographic factors also influence synthesis capacity independently of PD, but these effects are smaller than those accounted by PD. Synthesis capacity (1) declined with aging and particularly after the age of around 50, (2) was higher in females than males, yet not in PD patients alone, and (3) showed a possible association with BMI in striatal regions. Although thalamic findings were uncertain, they were mainly consistent with the overall pattern in the striatum.

The dopamine synthesis capacity was positively correlated across striatal and thalamic regions in both healthy controls and PD patients, suggesting a relatively uniform interregional effect. In a limited dual-tracer subsample that likely overrepresented late-stage PD, we observed a positive correlation between dopamine synthesis capacity and D_2R availability in caudate, yet no clear associations in the other regions.

Methodologically, scanner had a substantial influence on Ki^{ref} estimates, emphasizing the need to adjust for scanner effects in multi-scanner datasets. When MRI is unavailable, atlas-based normalization may be used to prevent data loss, though MRI-based normalization should remain the preferred approach.

CRediT authorship contribution statement

Tuulia Malén: Writing – review & editing, Writing – original draft, Visualization, Validation, Project administration, Methodology, Funding acquisition, Formal analysis, Data curation, Conceptualization. **Jouni Tuisku:** Writing – review & editing, Visualization, Validation, Software, Methodology, Formal analysis, Data curation. **Marco Bucci:** Writing – review & editing, Validation, Software, Methodology, Data curation, Conceptualization. **Severi Santavirta:** Writing – review & editing, Visualization, Validation, Methodology, Conceptualization. **Valtteri Kaasinen:** Writing – review & editing, Resources, Investigation, Data curation, Conceptualization. **Sakari Kaasalainen:** Writing – review & editing, Resources, Investigation, Data curation. **Janne Isojärvi:** Writing – review & editing, Software, Data curation. **Jarmo Hietala:** Writing – review & editing, Resources, Investigation. **Juha Rinne:** Writing – review & editing, Resources, Investigation. **Lauri Nummenmaa:** Writing – review & editing, Visualization, Supervision, Resources, Investigation, Formal analysis, Conceptualization.

Ethics approval

Finnish legislation does not require ethical approval for register-based studies.

Declaration of competing interest

The authors declare that they have no known competing financial interests or personal relationships that could have appeared to influence the work reported in this paper.

Acknowledgements

Funding: This work was supported by the Finnish Cultural Foundation; the Finnish Governmental Research Funding for Turku University Hospital and for the Western Finland collaborative area; the Päivikki and Sakari Sohlberg Foundation; and the Finnish Brain Foundation (grants to Malén). We acknowledge the following experts on the field for their consultancy: Senior Research Fellow and modeling specialist Vesa Oikonen (Patlak modeling), Postdoctoral Researcher Filip Grill (literature and visualization), Professor Sven De Maeyer from the University of Antwerp, Belgium, and data engineer and scientist Tomi Karjalainen (Bayesian regression modeling and visualization). Finally, we thank Tuomas Knuuti, Lilli Laine, Veera Soininen, and Jenny Lindman for conducting quality control for the preprocessed imaging data and Heidi Laine for language checking.

Appendix A. Supplementary data

Supplementary data to this article can be found online at https://doi.org/10.1016/j.nicl.2026.103944.

Data availability

The mean brain maps of group specific (healthy controls and PD patients) dopamine synthesis capacities are available in NeuroVault (https://neurovault.org/collections/OKUNGLWA/).

References

Antonini, A., Vontobel, P., Psylla, M., Günther, I., Maguire, P.R., Missimer, J., Leenders, K.L., 1995. Complementary positron emission tomographic studies of the striatal dopaminergic system in Parkinson's disease. Arch. Neurol. 52 (12), 1183–1190. https://doi.org/10.1001/archneur.1995.00540360061017.

Auguie, B., 2017. gridExtra: Miscellaneous Functions for "Grid" Graphics. doi:10.32614/CRAN.package.gridExtra.

Berry, A.S., Shah, V.D., Furman, D.J., White III, R.L., Baker, S.L., O'Neil, J.P., Janabi, M., D'Esposito, M., Jagust, W.J., 2018. Dopamine synthesis capacity is associated with D2/3 receptor binding but not dopamine release. Neuropsychopharmacology 43 (6), 1201–1211. https://doi.org/10.1038/npp.2017.180.

Bürkner, P.-C., 2017. brms: an R package for Bayesian multilevel models using Stan. J. Stat. Softw. 80 (1), 1–28. https://doi.org/10.18637/jss.v080.i01.

Bürkner, P.-C., 2018. Advanced Bayesian multilevel modeling with the R package brms. R Journal 10 (1). https://doi.org/10.32614/RJ-2018-017.

Bürkner, P.-C., 2021. Bayesian item response modeling in R with brms and Stan. J. Stat. Softw. 100 (5), 1–54. https://doi.org/10.18637/jss.v100.i05.

Cheng, H.C., Ulane, C.M., Burke, R.E., 2010. Clinical progression in Parkinson disease and the neurobiology of axons. Ann. Neurol. 67 (6), 715–725. https://doi.org/10.1002/ana.21995.

Cropley, V.L., Fujita, M., Bara-Jimenez, W., Brown, A.K., Zhang, X.-Y., Sangare, J., Herscovitch, P., Pike, V.W., Hallett, M., Nathan, P.J., 2008. Pre-and post-synaptic dopamine imaging and its relation with frontostriatal cognitive function in Parkinson disease: PET studies with [11C] NNC 112 and [18F] FDOPA. Psychiatry Res. Neuroimaging 163 (2), 171–182. https://doi.org/10.1016/j.pscychresns.2007.11.003.

Cumming, P., Wong, D.F., Dannals, R.F., Gillings, N., Hilton, J., Scheffel, U., Gjedde, A., 2002. The competition between endogenous dopamine and radioligands for specific binding to dopamine receptors. Ann. N. Y. Acad. Sci. 965 (1), 440–450. https://doi.org/10.1111/j.1749-6632.2002.tb04185.x.

Darbin, O., 2012. The aging striatal dopamine function. Parkinsonism Relat. Disord. 18 (5), 426–432. https://doi.org/10.1016/j.parkreldis.2011.11.025.

de la Fuente-Fernández, R., 2012. Frontostriatal cognitive staging in Parkinson's disease. Parkinson's Dis. 2012 (1), 561046. https://doi.org/10.1155/2012/561046.

Dowle, M.S., Arun. (2023). data.table: Extension of 'data.frame'. doi:10.32614/CRAN.package.data.table.

Elsinga, P.H., Hatano, K., Ishiwata, K., 2006. PET tracers for imaging of the dopaminergic system. Curr. Med. Chem. 13 (18), 2139–2153. https://doi.org/10.2174/092986706777935258.

Fischl, B., 2012. FreeSurfer. NeuroImage 62 (2), 774–781. https://doi.org/10.1016/j.neuroimage.2012.01.021.

Fortin, J.-P., Parker, D., Tunç, B., Watanabe, T., Elliott, M.A., Ruparel, K., Roalf, D.R., Satterthwaite, T.D., Gur, R.C., Gur, R.E., 2017. Harmonization of multi-site diffusion tensor imaging data. Neuroimage 161, 149–170. https://doi.org/10.1016/j.neuroimage.2017.08.047.

Gibb, W., Lees, A., 1988. The relevance of the Lewy body to the pathogenesis of idiopathic Parkinson's disease. J. Neurol. Neurosurg. Psychiatry 51 (6), 745–752. https://doi.org/10.1136/jnnp.51.6.745.

Gjedde, A., Reith, J., Dyve, S., Léger, G., Guttman, M., Diksic, M., Evans, A., Kuwabara, H., 1991. Dopa decarboxylase activity of the living human brain. Proc. Natl. Acad. Sci. 88 (7), 2721–2725. https://doi.org/10.1073/pnas.88.7.2721.

Haaxma, C.A., Bloem, B.R., Borm, G.F., Oyen, W.J., Leenders, K.L., Eshuis, S., Booij, J., Dluzen, D.E., Horstink, M.W., 2007. Gender differences in Parkinson's disease. J. Neurol. Neurosurg. Psychiatry 78 (8), 819–824. https://doi.org/10.1136/jnnp.2006.103788.

Janssen, L.K., Horstmann, A., 2022. Molecular imaging of central dopamine in obesity: a qualitative review across substrates and radiotracers. Brain Sci. 12 (4), 486. https://doi.org/10.3390/brainsci12040486.

Joutsa, J., Voon, V., Johansson, J., Niemelä, S., Bergman, J., Kaasinen, V., 2015. Dopaminergic function and intertemporal choice. Transl. Psychiatry 5 (1), e491–e. https://doi.org/10.1038/tp.2014.133.

Kaasinen, V., Vahlberg, T., 2017. Striatal dopamine in Parkinson disease: a meta-analysis of imaging studies. Ann. Neurol. 82 (6), 873–882. https://doi.org/10.1002/ana.25103.

Kaasinen, V., Vahlberg, T., Stoessl, A.J., Strafella, A.P., Antonini, A., 2021. Dopamine receptors in Parkinson's disease: a meta-analysis of imaging studies. Mov. Disord. https://doi.org/10.1002/mds.28632.

Kalia, L.V., Lang, A.E., 2015. Parkinson's disease. Lancet 386 (9996), 896–912. https://doi.org/10.1016/S0140-6736(14)61393-3.

Karjalainen, T., Tuisku, J., Santavirta, S., Kantonen, T., Bucci, M., Tuominen, L., Hirvonen, J., Hietala, J., Rinne, J.O., Nummenmaa, L., 2020. Magia: robust automated image processing and kinetic modeling toolbox for PET neuroinformatics. Front. Neuroinf. 14, 3. https://doi.org/10.3389/fninf.2020.00003.

Karrer, T.M., Josef, A.K., Mata, R., Morris, E.D., Samanez-Larkin, G.R., 2017. Reduced dopamine receptors and transporters but not synthesis capacity in normal aging adults: a meta-analysis. Neurobiol. Aging 57, 36–46. https://doi.org/10.1016/j.neurobiolaging.2017.05.006.

Kay, M., 2023a. ggdist: Visualizations of Distributions and Uncertainty. doi:10.5281/zenodo.3879620.

Kay, M., 2023b. tidybayes: Tidy Data and Geoms for Bayesian Models. doi:10.5281/zenodo.1308151.

Laakso, A., Vilkman, H., Örgen Bergman, J., Haaparanta, M., Solin, O., Syvälahti, E., Salokangas, R.K., Hietala, J., 2002. Sex differences in striatal presynaptic dopamine synthesis capacity in healthy subjects. Biol. Psychiatry 52 (7), 759–763. https://doi.org/10.1016/S0006-3223(02)01369-0.

Lee, J.J., Ham, J.H., Lee, P.H., Sohn, Y.H., 2015. Gender differences in age-related striatal dopamine depletion in Parkinson's disease. J. Movement Disord. 8 (3), 130. https://doi.org/10.14802/jmd.15031.

Lee, Y., Kroemer, N.B., Oehme, L., Beuthien-Baumann, B., Goschke, T., Smolka, M.N., 2018. Lower dopamine tone in the striatum is associated with higher body mass index. Eur. Neuropsychopharmacol. 28 (6), 719–731. https://doi.org/10.1016/j.euroneuro.2018.03.009.

Lövdal, S., van Veen, R., Carli, G., Renken, R., Shiner, T., Bregman, N., Orad, R., Arnaldi, D., Orso, B., Morbelli, S., 2025. IRMA: machine learning-based harmonization of $${\,}^{18} $$ F-FDG PET brain scans in multi-center studies. Eur. J. Nucl. Med. Mol. Imaging 52 (8), 2941–2958. https://doi.org/10.1007/s00259-025-07114-4.

Malén, T., Karjalainen, T., Isojärvi, J., Vehtari, A., Bürkner, P.-C., Putkinen, V., Kaasinen, V., Hietala, J., Nuutila, P., Rinne, J., 2022. Atlas of type 2 dopamine receptors in the human brain: age and sex dependent variability in a large PET cohort. Neuroimage 255, 119149. https://doi.org/10.1016/j.neuroimage.2022.119149.

Malén, T., Santavirta, S., De Maeyer, S., Tuisku, J., Kaasinen, V., Kankare, T., Isojärvi, J., Rinne, J., Hietala, J., Nuutila, P., 2024. Alterations in type 2 dopamine receptors across neuropsychiatric conditions: a large-scale PET cohort. NeuroImage: Clinical 103578. https://doi.org/10.1016/j.nicl.2024.103578.

McElreath, R., 2020. Statistical Rethinking: A Bayesian Course With Examples in R and Stan, second ed. Chapman and Hall/CRC.

Nurmi, E., Ruottinen, H.M., Bergman, J., Haaparanta, M., Solin, O., Sonninen, P., Rinne, J.O., 2001. Rate of progression in Parkinson's disease: a 6-[18F] fluoro-L-dopa PET study. Mov. Disord. 16 (4), 608–615. https://doi.org/10.1002/mds.1139.

Pak, K., Nummenmaa, L., 2023. Brain Dopamine Receptor System is Not Altered in Obesity: Bayesian and Frequentist Meta-Analyses. *medRxiv*, 2023.2006.2022.23291735. doi:10.1002/hbm.26534.

Patlak, C.S., Blasberg, R.G., 1985. Graphical evaluation of blood-to-brain transfer constants from multiple-time uptake data. Generalizations. J. Cereb. Blood Flow Metab. 5 (4), 584–590. https://doi.org/10.1038/jcbfm.1985.87.

Pavese, N., Rivero-Bosch, M., Lewis, S.J., Whone, A.L., Brooks, D.J., 2011. Progression of monoaminergic dysfunction in Parkinson's disease: a longitudinal 18F-dopa PET study. Neuroimage 56 (3), 1463–1468. https://doi.org/10.1016/j.neuroimage.2011.03.012.

Pedersen, T.L., 2024. patchwork: The Composer of Plots. doi:10.32614/CRAN.package.patchwork.

Pohjalainen, T., Rinne, J.O., Någren, K., Syvälahti, E., Hietala, J., 1998. Sex differences in the striatal dopamine D2 receptor binding characteristics in vivo. Am. J. Psychiatry 155 (6), 768–773. https://doi.org/10.1176/ajp.155.6.768.

Posit team. (2023). RStudio: Integrated Development Environment for R. https://posit.co.

Postuma, R.B., Berg, D., Stern, M., Poewe, W., Olanow, C.W., Oertel, W., Obeso, J., Marek, K., Litvan, I., Lang, A.E., 2015. MDS clinical diagnostic criteria for Parkinson's disease. Mov. Disord. 30 (12), 1591–1601. https://doi.org/10.1002/mds.26424.

R Core Team. (2025). R: A Language and Environment for Statistical Computing. https://www.R-project.org.

Rinne, J.O., Laihinen, A., Ruottinen, H., Ruotsalainen, U., Någren, K., Lehikoinen, P., Oikonen, V., Rinne, U., 1995. Increased density of dopamine D2 receptors in the putamen, but not in the caudate nucleus in early Parkinson's disease: a PET study with [11C] raclopride. J. Neurol. Sci. 132 (2), 156–161. https://doi.org/10.1016/0022-510x(95)00137-q.

Rorden, C., 2025. MRIcroGL: voxel-based visualization for neuroimaging. Nat. Methods 22 (8), 1613–1614. https://doi.org/10.1038/s41592-025-02763-7.

Samii, A., Markopoulou, K., Wszolek, Z., Sossi, V., Dobko, T., Mak, E., Calne, D., Stoessl, A.J., 1999. PET studies of Parkinsonism associated with mutation in the α-synuclein gene. Neurology 53 (9), 2097. https://doi.org/10.1212/WNL.53.9.2097.

Sossi, V., Holden, J., De la Fuente-Fernandez, R., Ruth, T., Stoessl, A., 2003. Effect of dopamine loss and the metabolite 3-O-methyl-[18F] fluoro-dopa on the relation between the 18F-fluorodopa tissue input uptake rate constant Kocc and the [18F] fluorodopa plasma input uptake rate constant Ki. J. Cereb. Blood Flow Metab. 23 (3), 301–309. https://doi.org/10.1097/01.WCB.0000050041.22945.3E.

Stan Development Team. (2023). RStan: the R interface to Stan. https://mc-stan.org/.

The MathWorks Inc. MATLAB [Computer software], Natick, Massachusetts: The MathWorks Inc. https://www.mathworks.com.

Thobois, S., Vingerhoets, F., Fraix, V., Xie-Brustolin, J., Mollion, H., Costes, N., Mertens, P., Benabid, A.-L., Pollak, P., Broussolle, E., 2004. Role of dopaminergic treatment in dopamine receptor down-regulation in advanced Parkinson disease: a positron emission tomographic study. Arch. Neurol. 61 (11), 1705–1709. https://doi.org/10.1001/archneur.61.11.1705.

Vehtari, A., Gelman, A., Simpson, D., Carpenter, B., Bürkner, P.-C., 2021. Rank-normalization, folding, and localization: an improved R for assessing convergence of MCMC. Bayesian Anal. 1 (1), 1–28. https://doi.org/10.1214/20-BA1221.

Volkow, N.D., Fowler, J.S., Gatley, S.J., Logan, J., Wang, G.-J., Ding, Y.-S., Dewey, S., 1996. PET evaluation of the dopamine system of the human brain. J. Nucl. Med. 37 (7), 1242–1256.

Wallace, D.L., Aarts, E., Dang, L.C., Greer, S.M., Jagust, W.J., D′ Esposito, M., 2014. Dorsal striatal dopamine, food preference and health perception in humans. PLoS One 9 (5), e96319. https://doi.org/10.1371/journal.pone.0096319.

Wickham, H., 2007. Reshaping data with the reshape package. J. Stat. Softw. 21, 1–20. https://doi.org/10.18637/jss.v021.i12.

Wickham, H., 2016. ggplot2: Elegant Graphics for Data Analysis. https://ggplot2.tidyverse.org.

Wickham, H., 2021. tidyr: Tidy Messy Data. R package version 1.1.3. doi:10.32614/CRAN.package.tidyr.

Wickham, H., 2022. stringr: Simple, Consistent Wrappers for Common String Operations. doi:10.32614/CRAN.package.stringr.

Wickham, H. F., Romain; Henry, Lionel; Müller, Kirill; Vaughan, Davis. (2023). dplyr: a grammar of data manipulation. doi:10.32614/CRAN.package.dplyr.

Wickham, H.S., Dana, 2022. scales: Scale Functions for Visualization. doi:10.32614/CRAN.package.scales.

Wilcox, C.E., Braskie, M.N., Kluth, J.T., Jagust, W.J., 2010. Overeating behavior and striatal dopamine with 6-[18F]-Fluoro-L-m-tyrosine PET. J. Obes. 2010 (1), 909348. https://doi.org/10.1155/2010/909348.